Impact of future land cover changes on HNO$_3$ and O$_3$ surface dry deposition.

T. Verbeke[1], J. Lathière[1], S. Szopa[1], N. de Noblet-Ducoudré[1]

[1] {Laboratoire des Sciences du Climat et de l'Environnement - LSCE-IPSL, CEA/CNRS/UVSQ, Gif-sur-Yvette, France}

Correspondence to: J. Lathière (juliette.lathiere@lsce.ipsl.fr)

Abstract

Dry deposition is a key component of surface-atmosphere exchange of compounds, acting as a sink for several chemical species. Meteorological factors, chemical properties of the trace gas considered and land surface properties are strong drivers of dry deposition efficiency and variability. Under both climatic and anthropogenic pressure, the vegetation distribution over the Earth has been changing a lot over the past centuries, and could be significantly altered in the future. In this study, we perform a modeling investigation of the potential impact of land-cover changes between present-day (2006) and the future (2050) on dry deposition velocities at the surface, with special interest for ozone (O$_3$) and nitric acid (HNO$_3$), two compounds which are characterized by very different physico-chemical properties. The 3D chemistry transport model LMDz-INCA is used, considering changes in vegetation distribution based on the three future projections RCPs 2.6, 4.5 and 8.5, and present-day (2007) meteorology. The 2050 RCP 8.5 vegetation distribution leads to a rise by up to 7% (+0.02 cm/s) in the surface deposition velocity calculated for ozone (V$_{d,O_3}$) and a decrease of -0.06 cm/s in the surface deposition velocity calculated for nitric acid (V$_{d,HNO_3}$) relative to the present day values in tropical Africa, and up to +18% and -15% respectively in Australia. When taking into account the RCP 4.5 scenario, which shows dramatic land cover change in Eurasia, V$_{d,HNO_3}$ increases by up to 20% (annual-mean value) and reduces V$_{d,O_3}$ by the same magnitude in this region. When analyzing the impact of

surface dry deposition change on atmospheric chemical composition, our model calculates that the effect is lower than 1 ppb on annual mean surface ozone concentration, for both the RCP8.5 and RCP2.6 scenarios. The impact on HNO_3 surface concentrations is more disparate between the two scenarios, regarding the spatial repartition of effects. In the case of the RCP 4.5 scenario, a significant increase of the surface O_3 concentration reaching locally by up to 5 ppb (+5%) is calculated on average during the June-August period. This scenario induces also an increase of HNO_3 deposited flux exceeding locally 10% for monthly values. Comparing the impact of land-cover change to the impact of climate change, considering a 0.93°C increase of global temperature, on dry deposition velocities, we estimate that the strongest increase over lands occurs in the North Hemisphere during winter especially in Eurasia, by +50% (+0.07 cm/s) for V_{d,O_3} and +100% (+0.9 cm/s) for V_{d,HNO_3}. However, different regions are affected by both changes, with climate change impact on deposition characterized by a latitudinal gradient, while the land-cover change impact is much more heterogeneous depending on vegetation distribution modification described in the future RCP scenarios. The impact of long-term land-cover changes on dry deposition is shown to be significant and to differ strongly from one scenario to another. It should therefore be considered in biosphere-atmospheric chemistry interaction studies in order to have a fully consistent picture.

1. Introduction

Amongst surface-atmosphere interactions, dry deposition plays a key role in the exchange of compounds and acts as a significant sink for several atmospheric species. Performing an intercomparison of 26 state-of-the-art atmospheric chemistry models, Stevenson et al. (2006) estimated the surface removal of ozone by dry deposition to be about 1000±200 Tg/yr on average, with values ranging from 720 to 1507 Tg/yr amongst models, compared to 5100, 4650 and 550 Tg/yr for chemical production, chemical destruction and stratospheric input fluxes respectively. This study also underlined that although global deposition fluxes are consistent between models, locally, there is a large variability in the ozone deposition velocities (Stevenson et al., 2006). Since all these models use deposition schemes based on Wesely's prescription (Wesely et al., 1989), the discrepancies suggest different hypotheses for the land-type consideration. Based on satellite measurements from OMI (Ozone Monitoring Instrument) combined with the Goddard Earth Observing System chemical transport model (GEOS-Chem),

58 Nowlan et al. 2014 estimated dry deposition to land to be 98% of total deposition for NO_2 and

59 33% for SO_2. This deposition fluxes over land represent 3% of global NOx emissions and 14% of

60 global sulfur emissions. Land surfaces can therefore play a significant role on deposition, with a

61 highly variable contribution from one chemical compound to another.

62 The air-surface exchange of trace compounds has been shown to be strongly variable, especially

63 between different types of surface vegetation and soil characteristics (Wesely et al., 2000).

64 Regarding ozone, model data differences reported in the literature could be attributed to

65 oversimplifications in the implementation of the dry deposition scheme (Val Martin et al. 2014)

66 since many models rely on "resistance in series" schemes developed in the 1980s (Hardacre et al.

67 2005).

68 In order to quantify the non-photochemical sink for tropospheric burden at the regional and

69 global scales, the scientific community uses numerical dry deposition schemes calibrated with

70 field-measurements of dry deposition velocities (Wesely et al., 1989, Zhang et al., 2002b),

71 implemented usually in chemistry-transport models. Dry deposition efficiency is influenced by

72 multiple meteorological factors (temperature, solar radiation, humidity and especially

73 atmospheric turbulence), chemical properties of the trace gas considered (solubility, oxidative

74 capacity), and land surface properties (surface type, surface roughness, foliar surface and

75 ecosystem height in the case of vegetation surfaces). Some of these factors are poorly constrained

76 and are thus accounted for in deposition schemes in a very simplistic way. The vegetation

77 distribution for instance is usually prescribed using maps for the region of interest that are

78 generally kept the same for either past, present or future studies (e.g. Andersson and Engardt,

79 2010 or Lamarque et al. 2013). There is therefore a lack of knowledge regarding the impact of

80 long-term changes in vegetation distribution on dry deposition chemical compounds at the

81 surface. Since the beginning of the industrial era, human activities have modified the use of large

82 surfaces, affecting significantly the vegetation distribution, especially in the northern temperate

83 latitude regions. Further land cover modifications are expected in the 21st century, due to

84 projected increases in energy and food demands, and vegetation, in tropical regions in particular,

85 could undergo drastic alterations.

86 Only a few studies have been carried out recently on the dry deposition changes in the future.

87 Some of them focus on the impact of climate change on the dry deposition (Andersson and

88 Engardt, 2010) while others combine the effects of several future changes (climate, CO_2 levels,

89   land cover) on atmospheric chemistry in general (Ganzeveld et al. 2010, Wu et al. 2012).
90   However, considering anthropogenic land cover changes among other large modifications of the
91   vegetation/atmospheric chemistry drivers does not allow to identify if the land cover change
92   should be or not considered as a priority in the studies of future atmospheric chemistry. The
93   objective of this study is to investigate and isolate the potential impact of land-cover changes
94   between the present-day (2006) and the future (2050) on dry deposition velocities at the surface,
95   using a modeling approach with a 3D chemistry transport model as illustrated in Figure 1.
96   Changes in vegetation distribution are based on the three future projections known as
97   Representative Concentration Pathways scenarios (RCPs) (van Vuuren et al. 2011), developed for
98   the climate model intercomparison project (CMIP5): RCPs 2.6, 4.5 and 8.5. For this work we
99   focus on ozone (O_3) and nitric acid (HNO_3), two compounds which are characterized by very
100 different biophysical properties (e.g. solubility and oxidative capacity). In section 2, we describe
101 the chemistry-transport model LMDz-INCA, the dry deposition module and the modeling
102 strategy adopted. In section 3, we describe the different future land cover changes as given in the
103 three RCP scenarios 2.6, 4.5 and 8.5, and explain their impacts on surface dry deposition
104 velocities of ozone and nitric acid. Finally, the magnitude of land cover effects related to climate
105 change on dry deposition velocities by 2050 is discussed.
106
107 **2. Modeling set up**
108 In our study, the global chemistry-climate model LMDz-INCA (Hauglustaine et al., 2004) is used
109 to compute dry deposition. LMDz (v4) is an atmospheric general circulation model that simulates
110 the transport of trace species. The model is run with 19 hybrid levels from the surface to 3hPa at
111 a horizontal resolution of 1.85° in latitude and 3.75° in longitude. It is coupled on-line to the
112 chemistry and aerosols model INCA (v2) which computes concentrations of reactive tracers
113 considering their emissions, chemical transformations, transport and deposition processes. The
114 atmospheric oxidation reactions of CH_4, CO and non-methane hydrocarbons are documented in
115 Folberth et al. (2006). In order to be able to isolate the effect of land-cover change only on the
116 atmospheric chemical composition, through change in surface dry deposition, emissions are
117 prescribed according to Lamarque et al. (2010) for anthropogenic fluxes and Lathière et al.
118 (2006) for biogenic VOCs, as described in Szopa et al. (2013), and are kept constant between all
119 runs.

120

2.1 Dry deposition in LMDz-INCA

The chemical deposition scheme used in INCA is based on the parameterization of Wesely (1989) and Wesely and Hicks (2000), computing dry deposition velocity V_d as a succession of resistances as follows:

$$|V_d(z)|=[R_a(z)+R_b+R_c]^{-1}$$

where R_a is the aerodynamic resistance, R_b the quasi-laminar resistance, and R_c the bulk surface resistance.

R_a determines the ability of the airflow to bring gases or particles close to the surface, and depends mainly on the atmospheric turbulence structure and on the height considered. In this paper, we will focus on dry deposition at the surface, ground level (z=0). R_b describes the resistance to the transfer very close to the surface and is driven by the surface (surface roughness) and the gas or particle (molecular diffusivity) characteristics. R_a and R_b are calculated based on Walcek et al. (1986). The surface resistance R_c represents the different pathways through which the gas or particles can deposit and is determined by the affinity of the surface for the chemical compound. Deposition can thus occurs directly on the ground and/or, in the case of vegetative surfaces, on the different vertical layers of the canopy on trunks, branches and mainly on leaves, through stomata or cuticles (Wesely, 1989). Vegetation surfaces in particular cover a large area of the Earth, with a high spatial and seasonal variability due to species diversity. Environmental conditions such as atmospheric CO_2 or pollutant (ozone) concentrations, radiation, temperature, or the occurrence of possible stress (drought for instance) can strongly affect the vegetation functioning, and the stomatal opening especially, and therefore impact dry deposition velocity. The impact of vegetation type, distribution and functioning, on dry deposition is still not well understood and generally very simply, if at all, considered in chemistry-transport models (Hardacre et al., 2015). For all chemical species considered in LMDz-INCA, R_c is based on their temperature dependent Henry's Law effective coefficient and reactivity factor for the oxidation of biological substances (Folberth et al., 2006). The coefficients for Henry's Law are taken from Sander (1999) and reactivity factors are taken from Wesely (1989) and Walmsley and Wesely (1996).

The dry deposition scheme implemented in LMDz-INCA considers eleven surface categories: (1) urban land, (2) agricultural land, (3) range land, (4) deciduous forest, (5) coniferous forest, (6)

5

151   mixed forest including wetland, (7) water, both salt and fresh, (8) barren land, mostly desert, (9)

152   non-forested wetland, (10) mixed agricultural and range land, and (11) rock open areas with low-

153   growing shrubs. This scheme was originally developed by Wesely (1989) and updated by Wesely

154   and Hicks (2000) for Northern hemisphere regions of United States and southern Canada regions.

155   Five seasonal categories are used as proxy of vegetation growth stage (midsummer with lush

156   vegetation; autumn with unharvested cropland; late autumn after frost, no snow; winter, snow on

157   ground, and subfreezing; transitional spring with partially green short annuals). For global scale

158   study purposes, the scheme in LMDz-INCA has been modified in order to represent the different

159   seasonal cycles throughout the world. The latitude dependency of the vegetation seasonality is

160   described by dividing the globe into three belts: Northern hemisphere regions (latitude > 33°N);

161   Tropical regions (33°S < latitude < 33°N) and Southern hemisphere regions (latitude < 33°S).

162   Summer is considered in the tropics throughout the whole year, describing the evergreen

163   vegetation. Two opposite seasonal cycles are taken into account in extra-tropical Northern and

164   Southern hemisphere regions, with winter being activated when snow falls. The deposition of

165   atmospheric compounds on plant leaves, through stomata especially, is determined following the

166   Wesely (1989) approach. The stomatal resistance depends on vegetation type, seasonal category,

167   radiation and temperature, but the potential impact of other environmental conditions such as

168   drought, or atmospheric concentration of CO_2 or ozone, are not considered. The dry deposition

169   velocity over each grid box is eventually determined by summing deposition velocities computed

170   over every land cover types, weighted by their respective fractional surface coverage (ranging

171   from 0 to 1).

172   The deposition velocities computed by LMDz-INCA based on a different land cover distribution

173   was evaluated in Hauglustaine et al. (2004). This work illustratesvalues generally consistent with

174   typical deposition velocities highlighted for North America and Europe as presented in Wesely

175   and Hicks (2000) and monthly values reaching up to 0.6 cm/s for ozone and up to 3 cm/s for

176   HNO_3 over land. In the supplementary material the ozone dry deposited fluxes simulated by

177   LMDz-INCA in the present-day simulation and used in this study are compared to other global

178   model and long term measurements which are discussed in Hardacre et al. (2015).

179

180   **2.2 Land use and land cover changes between 2007 and 2050**

181 The present-day distribution of vegetation categories considered in LMDz-INCA is illustrated in

182 Figure 2 as dominant type, covering the largest fraction of each gridbox. Crops are dominant

183 mainly in restricted temperate regions of North America, Central Europe, and also in India, while

184 range lands are largely spread. Deciduous forests dominate in tropical regions of South America,

185 Africa and Indonesia, together with Central and Southern Europe, while coniferous forests have a

186 high occupancy in boreal regions of North America and Eurasia. Figure 2 also shows the 10

187 regions of special interest selected for this study, which will be considered in more detail when

188 analyzing our results.

189 Future maps are based on scenarios of land-cover changes derived from four different

190 Representative Concentration Pathways (RCPs; Moss et al. 2010; Van vuuren et al. 2011) and

191 four Integrated Assessment Models (one per RCP) (RCP 8.5, RCP 4.5 and RCP 2.6). Those maps

192 were further harmonized to ensure smooth transitions with past/historical changes (Hurtt et al.

193 2011). Those datasets only provide information on human activities (crop land and grazed

194 pastureland) in each grid-cell (at a $0.5°$ resolution) but do not provide any recommendation

195 regarding the distribution of natural vegetation. We have therefore combined them with our

196 original present-day land-cover map (Loveland et al. 2000), which already includes both natural

197 and anthropogenic vegetation types, following a methodology described in Dufresne et al. (2013).

198 Figure 3 illustrates changes in vegetation fraction for agriculture and grasslands on one hand, and

199 for forests on the other hand, between present-day (distribution for 2007) and the future RCP

200 scenarios. For most affected regions, the changes in land surfaces are presented in Figure 4. The

201 RCP 4.5 scenario shows the largest surface change with a total of 20.8×10^6 km², representing

202 10.4% of the 70°S-70°N Earth continental surface. According to the RCP 2.6 and RCP 8.5

203 scenarios only 15 to 16.8×10^6 km² of land cover surfaces are converted.

204 The RCP 2.6 scenario is characterized by a moderate increase of energy consumption throughout

205 the 21st century together with a decrease in oil consumption. The energy supply is thus partly

206 ensured by bioenergy production increase (van Vuuren et al, 2011). Such hypotheses lead to a

207 strong expansion of agricultural lands ($+ 2.61 \times 10^6$ km² globally) at the expense of forests (- 1.40

208 $\times 10^6$ km²) and grasslands (- 1.15×10^6 km²) targeting mainly Eurasia, US and tropical southern

209 America.

210 The RCP 8.5 scenario, characterized by the strongest increase in population and energy

211 consumption, amongst RCPs), assumes a large increase in global population until 2050. The

212   resulting demand for food leads to a strong expansion of land used for crops and pastures at the

213   expense of forests. The tropical belt (from 30°N to 30°S) undergoes the largest changes: tropical

214   forests in southern America and southern Africa are partially harvested (1.0 x 10^6 km² totally, i.e.

215   13% of their 2007 extent) and replaced by grassland and crops, while in Eastern Australia, forests

216   lose 7% (- 0.28 x 10^6 km²) of their 2007 area and are replaced by grasslands which gains 0.12 x

217   10^6 km² on desert.

218   The "mitigation" RCP 4.5 scenario is a rather contrasting scenario as it proposes a strong increase

219   in the cover of all forest categories, a small expansion of grasslands but an important recession of

220   agricultural surfaces mainly in developed countries. Indeed Eurasia, US and Canada undergo a

221   strong conversion from agriculture and grassland to forests with a magnitude change of ~0.8 x

222   10^6 km² in Eurasia and ~0.4 x 10^6 km² in northern US and Canada. Besides, tropical southern

223   America loses 0.55 x 10^6 km² of cumulated croplands and grasslands but forests expand by the

224   same surface between present day and 2050.

225   Finally, it is important to underline that the 3 RCP scenarios offer a wide variety of land cover

226   change projections. They all are quite different compared to previous scenarios, such as the

227   SRES-A2 investigated by Ganzeveld et al. (2010), characterized by a strong North/South

228   contrast, with the tropical and southern hemisphere countries mainly encountering deforestation

229   whereas northern areas (>35°N) were mainly projected to see afforestation.

230

2.3 Simulation strategy

232   In order to quantify the effects of these land cover changes on surface dry deposition, we carried

233   out two sets of simulations (Table 1). The first set intends to isolate the effect of future possible

234   land cover changes on dry deposition without any climate change. It includes one control run

235   (present day), using 2006 vegetation distribution (Figure 2) and three future runs using the 2050

236   vegetation maps according to the RCPs 8.5, 4.5 and 2.6 scenarios. The same present-day

237   meteorology, biogenic and anthropogenic emissions are used in these four simulations. These

238   simulations are run for 1 year with wind and temperature fields being relaxed towards the

239   ECMWF ERA-interim reanalysis (Dee et al., 2011) with a time constant of 6 hours.

240   Then a second set of two simulations is performed in order to investigate the effect of future

241   climate change on deposition and compare it with the impact of future land cover change: one run

242   for the 2000-2010 period and a second run for the 2045-2055 period. Those simulations are

243 performed without nudging and the LMDz general circulation model requires sea surface

244 temperature (SST), solar constant and Long-Lived Green House Gases (LL-GHG) global mean

245 concentrations as forcings. For historical simulations, we use the HADiSST for sea surface

246 temperature (Rayner et al., 2003) and the evolution of LL-GHG concentrations compiled in the

247 AR4-IPCC report. For future projections, we use the SST from IPSL-CM4 simulation for the

248 SRES-A2 scenario, which induce similar climate trajectories in terms of radiative forcing than

249 RCP8.5. We use the LL-GHG concentrations distributed by the RCP database for RCP8.5

250 projection for the 2045-2055 period. Eleven years are run and averaged to allow smoothing of

251 interannual climate variability. The mean surface temperature change is 0.93°C between future

252 simulation and present day simulation. Both experiments use the same present-day vegetation

253 distribution, anthropogenic and biogenic emissions.

254

255 **3. Results**

256 **3.1. Present day ozone and nitric acid deposition**First of all, we present the deposition

257 over continental regions for present-day conditions (Figure 5) by illustrating the annual means of

258 deposition velocities at the surface, surface concentrations and deposited fluxes for O_3 and HNO_3.

259 The highest ozone deposition velocities (>0.35 cm/s) are simulated over India, south-eastern

260 Asia, western coast and center of South America, Mexico, Europe and sub Saharan Africa and

261 Australia. Hence, those areas are mainly covered by crops and grasses, where the highest V_{d,O_3}

262 occurs, while Europe and Southeast Asia are mainly covered by deciduous forests, with therefore

263 lower annual V_{d,O_3}. O_3 surface dry deposition is indeed maximal over small canopies vegetation

264 and minimal over bare soil with deposition affinity ranging from Agriculture > Grasslands >

265 Deciduous > Coniferous > Bare soil (see sensitivity tests in supplementary material).

266 Temperate regions see ozone deposition velocities significantly reduced in winter (see

267 supplementary material for seasonal means) whereas tropical regions, covered mainly by small

268 canopies, are characterized by surface deposition velocity exceeding 0.35 cm/s throughout the

269 whole year due to the lack of seasonality in the vegetation phenology in the global model. In

270 temperate regions of the Northern hemisphere, the highest deposition velocities for ozone reach

271 values of 0.4 cm/s to 0.6 cm/s for V_{d,O_3} over Europe.

272 For HNO_3, the annual mean deposition velocities are maximum over Brazil, Western Europe,

273 India, Indochinese Peninsula and South of western Africa (> 1.6 cm/s in annual mean). V_{d,HNO_3}

274   reaches maximum values over deciduous and coniferous forests, due to deposition affinity

275   ranking from: Deciduous, Coniferous > Agriculture > Grasslands > Bare soil. This is due to the

276   strong dependency of V_{d,HNO_3} to surface roughness (Walcek et al., 1986). For temperate region

277   and South Asia, the HNO_3 deposition is strongly affected by the vegetation cycle with maximum

278   in July between 2.5 cm/s and 3.5 cm/s. This is remarkable over temperate and boreal forests. In

279   the tropics, Amazonian forest encounters high HNO_3 deposition velocity in winter whereas

280   deposition velocity over African equatorial forest is limited throughout the whole year. (see

281   supplementary material for seasonal means of deposition). Large areas receive high HNO_3

282   deposition fluxes exceeding $0.5g(N)/m^2/yr$ in annual mean: North eastern USA, western Europe

283   and East Asia. These areas correspond to the ones identified by Dentener et al. 2006 and in which

284   natural vegetation encounters nitrogen deposition higher than the "critical load" threshold of

285     $1g(N)/m^2/yr$.

286   The repartition of deposited fluxes is strongly affected by the large variability of atmospheric

287   concentrations of ozone and nitric acid in the surface layer. For both O_3 and HNO_3, the deposited

288   fluxes are maximum over South and East Asia and eastern North America and central and

289   western Europe. For ozone, the maximum in winter is over central Africa whereas in summer the

290   ozone deposition is maximum over central Europe and eastern US. For HNO_3, the deposited flux

291   repartition is equally driven by the deposition velocity and by the HNO_3 surface concentration

292   distribution. In winter, HNO_3 is maximally deposited over eastern US, central Africa, central

293   Europe India and East Asia. In summer, regions are the same in the Northern hemisphere but the

294   extension of deposited HNO_3 areas is higher and the deposition in Africa is weak, due to weak

295   HNO_3 concentration.

296

297   **3.2. Impact of 2050-2007 land cover changes on surface dry deposition velocities.**

298   We then analyze the changes in surface dry deposition velocities between present day and 2050

299   induced only by land cover change. Four regions undergo interesting land cover changes in terms

300   of intensity or contrast between scenarios: Eurasia, North America, tropical Africa and Australia.

301   The left columns of Figures 6 and 7 show the relative difference in surface dry deposition

302   velocities distribution for O_3 and HNO_3, resulting from the changes in vegetation distribution

303   between 2007 and 2050 for the 3 RCP scenarios. We shall first describe the two scenarios

304   projecting weak land cover changes for 2050s: RCP8.5 and RCP2.6. In the RCP 8.5 scenario, one

305   main land cover change is the expansion of agricultural land at the expenses of forests. According

306   to this scenario, over tropical Africa, the maximal land cover change occurs locally with fraction

307   of deciduous forests decreasing by up to 0.2 while cropland fraction increases by up to 0.2 in the

308   same region. This induces a rise by up to 7% (+0.02 cm/s) in V_{d,O_3} and a decrease of 0.06 cm/s in

309   V_{d,HNO_3} relative to the present day values in this area. These order of magnitude and sign of

310   changes are consistent with sensitivity tests in which we replaced totally forests by croplands

311   inducing an increase of 0.1 cm/s in V_{d,O_3} and a decrease of 0.5 cm/s in V_{d,HNO_3} (during summer

312   and winter). The strongest LCC occurs in Australia (-0.12 in forest fraction and +0.2 in grassland

313   fraction in eastern Australian regions), which induces a local maximum increase of 18% (+0.05

314   cm/s) in V_{d,O_3} and a maximum decrease of 15% in V_{d,HNO_3} (-0.1 cm/s). We find the same order of

315   magnitude in changes induced by land cover change in Western Australia but with a different sign

316   for V_{d,HNO_3} changes (+0.1cm/s ; +9%), due to a different type of shift in surface covering (+0.12

317   in grassland fraction, -0.10 for desert).

318   As land cover changes are weak in the RCP 2.6 scenario, a more dispersed and weaker effect on

319   surface dry deposition velocities is simulated (maximum absolute difference of 10%).

320   According to the RCP 4.5 scenario, the most dramatic land cover change occurs in Eurasia where

321   local maximum changes by up to 0.5 in fraction of vegetation are projected, involving in most

322   cases an increase in forest surfaces at the expense of agricultural areas. This increases V_{d,HNO_3} by

323   up to 20% (annual-mean value) and reduces V_{d,O_3} by the same magnitude in this region. The LCC

324   impacts are stronger by a factor 4 to 6 in summer both on O_3 and HNO_3 deposition velocities.

325   This difference in deposition velocities between winter and summer were highlighted in

326   sensitivity tests which see a strong decrease in V_{d,O_3} during the June-August period (up to 0.15

327   cm/s in absolute) and a strong increase in V_{d,HNO_3} (up to 1.5 cm/s) underlining a total conversion

328   of croplands to forests. This is due to a higher surface roughness which enhances the deposition

329   velocity of HNO_3 (via the reduction of the aerodynamic resistance). However, the higher input

330   surface resistance (prescribed in the model and variable relating to season indexes) reduces V_{d,O_3}

331   even combined to a warmer climate which decreases the stomatal resistance (Rs).

332

333   **3.3. Impact on atmospheric composition**

The objective of this part is to isolate the effects of dry deposition changes due to land cover changes on the tropospheric concentration of O_3 and HNO_3. Therefore, solely the impact of land cover changes on deposition at the surface is considered between the present-day and 2050 simulations. This impact on surface concentrations of O_3 and HNO_3 is shown in the right columns of Figures 6 and 7.

For both the RCP8.5 and RCP2.6 scenarios, the LCC effects through deposition are lower than 1 ppb on annual mean surface ozone concentrations. In term of relative difference, only the reduction of ozone over Australia when considering RCP8.5 hypotheses is exceeding 1%, reaching up to 5% at some points. The impact on HNO_3 surface concentrations is more disparate between the two scenarios when considering the spatial repartition of effects. The RCP8.5 scenario leads to local increase of HNO_3 due to the reduction in the deposition velocity. This HNO_3 increase is notable over Mexico, Brazil, western and South Africa (comprised in the 1-6% interval). Land cover change in Australia leads to an increase exceeding 7% in the east and a decrease reaching 5% in the west.

The RCP4.5 scenario induces the strongest impacts on deposition velocity with a reduction of V_{d,O_3} (-0.08 cm/s) occurring in Eurasia due a strong reduction in croplands occupancy (-0.6 in fraction of coverage) and a strong increase in forest distribution (+0.6 in fraction of coverage) between 2007 and 2050. It induces a significant increase of the surface O_3 concentration reaching locally by up to 5 ppb (+5%) on average during the June-August period. This scenario induces also an increase of the HNO_3 deposition flux exceeding locally 10% for monthly values. In Eurasia and eastern North America. It thus leads to a reduction in the HNO_3 concentration by 0.2 ppbv in Eurasia (-13%) and in North America (-8%), mainly due to changes in nitric acid velocities of +0.5 cm/s and +0.2 cm/s respectively.

3.4 Are the land cover induced changes significant compared with the climate change impact?

The impact of land-use changes on deposition can be compared to the one of climate in order to discuss their respective strength on deposition velocities. To this purpose, we consider a 0.93°C increase of global temperature, corresponding to the temperature increase projected in the RCP scenarios between the beginning and the middle of the 21st century. The figure 8 shows the impact of this climate change on the deposition velocity for O_3 and HNO_3. We see that the

365   strongest increase in surface dry deposition velocities over lands occurs in the North Hemisphere

366   during winter especially in Eurasia (+50% (+0.07 cm/s) for V_{d,O_3} and +100% (+0.9 cm/s) for

367   V_{d,HNO_3}). The climate effect on the deposition velocity by affecting stomatal resistance, sensitive

368   to surface temperature and solar irradiance, can locally reach values far more important than the

369   LCC. The Table 2 presents the effects of land cover change considering RCP4.5 projection and

370   climate change on deposition velocity averaged over 10 regions for O_3 and HNO_3. In several

371   regions, the effect of land cover change is of the same order of magnitude than the one of climate.

372   The modification in land cover affectation can thus amplify the climate change effect or, when

373   the sign is the opposite, counterbalances it.

374

4. Discussion and conclusions

376   Using the 2.6, 4.5 and 8.6 RCP scenarios for land-use change between 2000s and 2050s,

377   simulations were carried out with the global chemistry-transport model LMDz-INCA in order to

378   assess the impact of changes in vegetation distribution on the dry deposition of ozone and nitric

379   acid at the surface and on atmospheric composition.

380   Regarding vegetation distribution, the largest change at the global scale is given in the RCP 4.5

381   scenario (20.8 x 10^6 km²), with surface converted being 28% and 19% lower in the RCP 2.6 and

382   RCP 8.5 scenarios respectively. Projections show major changes in the Northern Hemisphere in

383   the case of RCP 4.5 scenario, while Australia and Africa are mostly affected in the RCP 8.5

384   scenario.

385   Vegetation type and surface being key drivers of surface dry deposition, any change in vegetation

386   distribution can potentially affect dry deposition velocity and therefore atmospheric chemical

387   composition. Considering the 2050 RCP 8.5 vegetation distribution leads to a rise by up to 7%

388   (+0.02 cm/s) in V_{d,O_3} and a decrease of 0.06 cm/s in V_{d,HNO_3} relative to the present day values in

389   tropical Africa, and up to +18% and -15% respectively in Australia. As land cover changes are

390   weak in the RCP 2.6 scenario, a more dispersed and weaker effect on surface dry deposition

391   velocities is simulated (maximum absolute difference of 10%) when considering the RCP 2.6

392   scenario, characterized by a moderate change in vegetation distribution compared to present-day.

393   When taking into account the RCP 4.5 scenario, which shows dramatic land cover change in

394   Eurasia, V_{d,HNO_3} increases by up to 20% (annual-mean value) and reduces V_{d,O_3} by the same

395   magnitude in this region. When analyzing the impact of dry deposition change on atmospheric

13

396 chemical composition, our model calculates that the effect is lower than 1 ppb at the grid box
397 scale on annual mean surface ozone concentration, for both of the RCP8.5 and RCP2.6 scenarios.
398 The impact on HNO_3 surface concentrations is more disparate between the two scenarios,
399 regarding the spatial repartition of effects. In the case of the RCP 4.5 scenario, a significant
400 increase of the surface O_3 concentration reaching locally up to 5 ppb (+5%) is calculated on
401 average during the June-August period. This scenario induces also an increase of HNO_3
402 deposited flux exceeding locally 10% for monthly values. Investigating the impact of climate
403 change, considering a 0.93°C increase of global temperature, on surface dry deposition velocities,
404 we calculate that the strongest increase over lands occurs in the North Hemisphere during winter
405 especially in Eurasia (+50% (+0.07 cm/s) for V_{d,O_3} and +100% (+0.9 cm/s) for V_{d,HNO_3}). The
406 climate change impact on deposition is characterized by a latitudinal gradient, while the effect of
407 land-cover change is much more heterogeneous. Both climate and vegetation distribution changes
408 are of similar amplitude but sign can differ.

409 The objective in this study is to isolate the impact of land-cover change on atmospheric chemical
410 composition through modification of surface dry deposition only rather than to consider
411 comprehensively all the atmospheric chemistry/vegetation interactions affected by land cover
412 change. Indeed, as far as long term evolution of atmospheric chemistry is investigated (e.g.
413 Stevenson et al. 2006, Lamarque et al. 2010), the evolution of biogenic emissions due to global
414 changes is discussed, if not shared between models, but the land cover maps used for dry
415 deposition remain unchanged. Here we want to assess the importance of this choice. Land cover
416 changes would go together with changes in surface emissions, either from anthropogenic,
417 agricultural, or biogenic sources, with changes in climate, and possible strong consequences on
418 the atmospheric chemical mechanism and surface-atmosphere interactions. In an attempt to
419 quantify all the effects of land cover change, those processes would therefore need to be
420 considered altogether to get a better picture of the overall resulting effect. However they all have
421 large uncertainties and added to error compensation effects, the dry deposition change can be can
422 masked by other process changed (see for example Wu et al., 2012). Moreover, the sensitivity of
423 biogenic emissions to climate and CO_2 changes as well as the level of coupling between
424 vegetation and chemistry are so different from one model to another that the full land cover
425 change response is for the moment highly model-dependent.

426 Fowler et al. (2009) underline an uncertainty of about 50% in the ability of models to estimate
427 dry deposition fluxes for main chemical species, the lack of measurements making a proper and
428 extensive model evaluation especially difficult. Hardacre et al. (2015), who compared the dry
429 deposition of ozone of 15 global atmospheric chemistry-transport models with measurements in
430 Europe and North America underline discrepancies of up to a factor of two, notably in the
431 summer maximum, but do not find a systematic model bias. Dry deposition in global models is
432 still largely based on the in-series resistance approach proposed by Wesely (1989) and generally
433 do not integrate more recent findings demonstrated by field or laboratory studies (Hardacre et al.,
434 2015).

435 Vegetation is usually crudely described in chemistry-transport models, with leaf surface or cuticle
436 and stomatal resistances for instance being prescribed or very simply parameterized, and lack of
437 the representation of seasonal variation or stress (water, temperature) impacts. This could lead to
438 significant uncertainty in model representation and projections of atmospheric chemical
439 composition and surface-atmosphere interactions. The work by Wesely and Hicks (2000)
440 underlines that selecting proper input parameters for dry deposition schemes, such as stomatal,
441 cuticle, and soil resistances, is crucial for a satisfactory determination of dry deposition
442 efficiency, for both simple and multi-layers models. Zhang et al. (2003) propose a revised
443 parameterization of dry deposition including the leaf area index in the calculation of aerodynamic
444 and cuticular resistances, which could give the possibility of a better representation of the impact
445 of vegetation seasonality in dry deposition estimates. The roles of surface wetness, soil moisture,
446 the partition between stomatal and non-stomatal uptake for instance, shown of high importance
447 for dry deposition processes, are usually not implemented or poorly described in global models
448 (Fowler et al., 2009; Hardacre et al., 2015). This is also the case of the LMDz-INCA model in
449 which dry deposition is described through a highly parameterized approach. Investigating ozone
450 non-stomatal uptake using measurements over five different vegetation types, Zhang et al.
451 (2002a) show that the O_3 uptake by cuticles is affected by friction velocity, relative humidity,
452 canopy wetness and LAI especially, and tends to increase with wetness and high humidity. A new
453 parameterization for non-stomatal uptake is proposed and is expected to improve this deposition
454 path in existing models, where a constant value is often considered, and could therefore be tested
455 more largely in global models. Investigating the impact of coupling dry deposition to vegetation
456 phenology in the Community Earth System Model (CESM) on ozone surface simulation, Val

457 Martin et al. (2014) show the importance of representing the dependence of dry deposition to
458 vegetation parameters including drivers of stomatal resistance variation (change in CO_2, drought
459 stress), especially when focusing on the impact of past or future changes of vegetation. Hardacre
460 et al. (2015) recommend to provide more detailed diagnostics of O_3 dry deposition in next
461 intermodel exercices to attribute the intermodal differences to methodology and/or representation
462 of processes. The next generation of chemistry-transport models should therefore rely on online
463 coupling with vegetation, with dry deposition schemes having a consistent and dynamic
464 description of vegetation distribution and growth and related short-term (seasonal, annual
465 variation) or long-term (past and future changes) evolutions. However, model intercomparisons
466 focusing on each process considered in isolation with a proper shared methodology/set-up is
467 crucial if one wants to progress in the understanding of the complex vegetation/atmospheric
468 chemistry interactions. In particular the evolution of land cover maps should be considered as far
469 as dry deposition is concerned in addition to emission changes in the next intermodel exercices
470 aiming to project future atmospheric chemistry.
471

References

Andersson, C. and Engardt, M.: European ozone in a future climate: Importance of changes in dry deposition and isoprene emissions, J. Geophys. Res.-Atmos., 115, D02303, doi:10.1029/2008JD011690, 2010.

Dentener, F., et al. (2006), Nitrogen and sulfur deposition on regional and global scales: A multimodel evaluation, Global Biogeochem. Cycles, 20, GB4003, doi:10.1029/2005GB002672.

Dee, D. P., Uppala, S. M., Simmons, A. J., Berrisford, P., Poli, P., Kobayashi, S., Andrae, U., Balmaseda, M. A., Balsamo, G., Bauer, P., Bechtold, P., Beljaars, A. C. M., van de Berg, L., Bidlot, J., Bormann, N., Delsol, C., Dragani, R., Fuentes, M., Geer, A. J., Haimberger, L., Healy, S. B., Hersbach, H., Hólm, E. V., Isaksen, L., Kållberg, P., Köhler, M., Matricardi, M., McNally, A. P., Monge-Sanz, B. M., Morcrette, J.-J., Park, B.-K., Peubey, C., de Rosnay, P., Tavolato, C., Thépaut, J.-N. and Vitart, F. (2011), The ERA-Interim reanalysis: configuration and performance of the data assimilation system. Q.J.R. Meteorol. Soc., 137: 553–597. doi: 10.1002/qj.828.

Dufresne, J.-L., Foujols, M.-A., Denvil, S., Caubel, A., Marti, O., Aumont, O., Balkanski, Y., Bekki, S., Bellenger, H., Benshila, R., Bony, S., Bopp, L., Braconnot, P., Brockmann, P., Cadule, P., Cheruy, F., Codron, F., Cozic, A., Cugnet, D., de Noblet, N., Duvel, J.-P., Ethé, C., Fairhead, L., Fichefet, T., Flavoni, S., Friedlingstein, P., Grandpeix, J.-Y., Guez, L., Guilyardi, E., Hauglustaine, D., Hourdin, F., Idelkadi, A., Ghattas, J., Joussaume, S., Kageyama, M., Krinner, G., Labetoulle, S., Lahellec, A., Lefebvre, M.-P., Lefevre, F., Levy, C., Li, Z.X., Lloyd, J., Lott, F., Madec, G., Mancip, M., Marchand, M., Masson, S., Meurdesoif, Y., Mignot, J., Musat, I., Parouty, S., Polcher, J., Rio, C., Schulz, M., Swingedouw, D., Szopa, S., Talandier, C., Terray, P., Viovy, N., Vuichard, N., Climate change projections using the IPSL-CM5 Earth System Model: from CMIP3 to CMIP5, Clim. Dynamics, 40, doi: 10.1007/s00382-012-1636-1, 2013.

Folberth, G. A., Hauglustaine, D. A., Lathière, J., and Brocheton, F.: Interactive chemistry in the Laboratoire de Météorologie Dynamique general circulation model: model description and

500 impact analysis of biogenic hydrocarbons on tropospheric chemistry, Atmos. Chem. Phys., 6,

501 2273-2319, doi:10.5194/acp-6-2273-2006, 2006.

502 Fowler, D., Pilegaard, K., Sutton, M. A., Ambus, P., Raivonen, M., Duyzer, J., Simpson, D.,

503 Fagerli, H., Fuzzi, S., Schjoerring, J. K., Granier, C., Neftel, A., Isaksen, I. S. A., Laj, P., Maione,

504 M., Monks, P. S., Burkhardt, J., Daemmgen, U., Neirynck, J., Personne, E., Wichink-Kruit, R.,

505 Butterbach-Bahl, K., Flechard, C., Tuovinen, J. P., Coyle, M., Gerosa, G., Loubet, B., Altimir, N.,

506 Gruenhage, L., Ammann, C., Cieslik, S., Paoletti, E., Mikkelsen, T. N., Ro-Poulsen, H., Cellier,

507 P., Cape, J. N., Horvath, L., Loreto, F., Niinemets, U., Palmer, P. I., Rinne, J., Misztal, P., Nemitz,

508 E., Nilsson, D., Pryor, S., Gallagher, M. W., Vesala, T., Skiba, U., Brueggemann, N.,

509 Zechmeister-Boltenstern, S., Williams, J., O'Dowd, C., Facchini, M. C., de Leeuw, G., Flossman,

510 A., Chaumerliac, N., and Erisman, J.W.: Atmospheric composition change: Ecosystems-

511 Atmosphere interactions, Atmos. Environ., 43, 5193–5267, doi:10.1016/j.atmosenv.2009.07.068,

512 2009.

513 Ganzeveld, L., Bouwman, L., Stehfest, E., Vuuren, D. P. V., Eickhout, B., and Lelieveld, J.:

514 Impact of future land use and land cover changes on atmospheric chemistry-climate interactions,

515 J. Geophys. Res., 115, D23301, doi:10.1029/2010JD014041, 2010.

516 Hardacre, C., Wild, O., and Emberson, L.: An evaluation of ozone dry deposition in global scale

517 chemistry climate models, Atmos. Chem. Phys., 15, 6419-6436, doi:10.5194/acp-15-6419-2015,

518 2015.

519 Hauglustaine, D.A., Hourdin, F., Jourdain, L ., Filiberti, M.A., Walters, S., Lamarque, J.-F. and

520 Holland, E.A.: Interactive chemistry in the Laboratoire de Meteorologie Dynamique general

521 circulation model: Description and background tropospheric chemistry evaluation, J. Geophys.

522 Res.-Atm., 109, D4, doi: D04314 10.1029/2003JD003957, 2004.

523 Hurtt, G. C., Chini, L. P., Frolking, S., Betts, R. A., Feddema, J., Fischer, G., Fisk, J. P., Hibbard,

524 K., Houghton, R. A., Janetos, A., Jones, C. D., Kindermann, G., Kinoshita, T., Goldewijk Kees

525 Klein Riahi, K. Shevliakova, E., Smith, S., Stehfest, E., Thomson, A., Thornton, P., van Vuuren,

526 D. P. and Wang, Y. P.: Harmonization of land-use scenarios for the period 1500-2100: 600 years

527 of global gridded annual land-use transitions, wood harvest, and resulting secondary lands,

528 Climatic Change, 109, 117-161, doi: 10.1007/s10584-011-0153-2, 2011.

529 Lamarque, J.-F., Bond, T. C., Eyring, V., Granier, C., Heil, A., Klimont, Z., Lee, D., Liousse, C.,

530 Mieville, A., Owen, B., Schultz, M. G., Shindell, D., Smith, S. J., Stehfest, E., Van Aardenne, J.,

531 Cooper, O. R., Kainuma, M., Mahowald, N., Mc-Connell, J. R., Naik, V., Riahi, K., and van

532 Vuuren, D. P.: Historical (1850–2000) gridded anthropogenic and biomass burning emissions of

533 reactive gases and aerosols: methodology and application, Atmos. Chem. Phys., 10, 7017–7039,

534 doi:10.5194/acp-10-7017-2010, 2010.

535 Lathière, J., Hauglustaine, D.A., De Noblet-Ducoudré, N., Krinner, G. and Folberth, G.A.: Past

536 and future changes in biogenic volatile organic compound emissions simulated with a global

537 dynamic vegetation model, Geophys. Res. Lett., 32, 20, doi: L20818 10.1029/2005GL024164,

538 2005.

539 Loveland, T. R., Reed, B. C., Brown, J. F., Ohlen, D. O., Zhu, Z., Yang, L., and Merchant, J. W.:

540 Development of a global land cover characteristics database and IGBP DISCover from 1 km

541 AVHRR data, Intern. J. Rem. Sens., 21(6–7), 1303–1330, 2000.

542 Moss, R.H., Edmonds, J.A., Hibbard, K.A., Manning, M.R., Rose, S.K., van Vuuren, D.P., Carter,

543 T.R., Emori, S., Kainuma, M., Kram, T., Meehl, G.A., Mitchell, J.F., Nakicenovic. N., Riahi, K.,

544 Smith, S.J., Stouffer, R.J., Thomson, A.M., Weyant, J.P. and Wilbanks, T.J.: The next generation

545 of scenarios for climate change research and assessment, Nature, 463, 7282, 747-756, doi:

546 10.1038/nature08823 FEB 11 2010, 2010.

547 Nowlan, C. R., Martin, R. V., Philip, S., Lamsal, L. N., Krotkov, N. A., Marais, E. A., Wang, S.

548 and Zhang, Q.: Global dry deposition of nitrogen dioxide and sulfur dioxide inferred from space-

549 based measurements, Global Biogeochem. Cy., 28, 1025–1043, doi:10.1002/2014GB004805,

550 2014.

551 Rayner, N.A., Parker, D.E., Horton, E.B., Folland, C.K., Alexander, L.V., Rowell, D.P., Kent,

552 E.C. and Kaplan, A.: Global analyses of sea surface temperature, sea ice, and night marine air

553 temperature since the late nineteenth century, J. of Geophys. Res.-Atm., 108, D14, 2156-2202,

554 doi: 10.1029/2002JD002670, 2003.

555 Sander, R.: Compilation of henry's law constants for inorganic and organic species of potential

556 importance in environmental chemistry (version 3), http://www.mpch-

557 mainz.mpg.de/sander/res/henry.html, 1999.

558 Stevenson, D.S., Dentener, F.J., Schultz, M.G., Ellingsen, K., van Noije, T.P.C., Wild, O., Zeng,

559 G., Amann, M., Atherton, C.S., Bell, N., Bergmann, D.J., Bey, I., Butler, T., Cofala, J., Collins,

560 W.J., Derwent, R.G., Doherty, R.M., Drevet, J., Eskes, H.J., Fiore, A.M., Gauss, M.,

561 Hauglustaine, D.A., Horowitz, L.W., Isaksen, I.S.A., Krol, M.C., Lamarque, J.F., Lawrence,

562 M.G., Montanaro, V., Muller, J.-F., Pitari, G., Prather, M.J., Pyle, J.A., Rast, S., Rodriguez, J.M.,

563 Sanderson, M.G., Savage, N.H., Shindell, D.T., Strahan, S.E., Sudo, K. and Szopa, S.:

564 Multimodel ensemble simulations of present-day and near-future tropospheric ozone, J. of

565 Geophys. Res.-Atm., 111, D8, doi: D08301 10.1029/2005JD006338, 2006.

566 Szopa, S., Balkanski, Y., Schulz, M., Bekki, S., Cugnet, D., Fortems-Cheiney, A., Turquety, S.,

567 Cozic, A., Deandreis, C., Hauglustaine, D., Idelkadi, A., Lathière, J., Lefèvre, F., Marchand, M.,

568 Vuolo, R., Yan, N. and Dufresne, J-L.: Aerosol and ozone changes as forcing for climate

569 evolution between 1850 and 2100, Climate Dynamics, 40, 9-10, 2223-2250, doi 10.1007/s00382-

570 012-1408-y, 2013.

571 Val Martin, M., Heald, C.L. and Arnold, S.R.: Coupling dry deposition to vegetation phenology

572 in the Community Earth System Model: Implications for the simulation of surface O_3, Geophys.

573 Res. Lett., 41, 2988–2996, doi:10.1002/2014GL059651, 2014.

574 van Vuuren, D.P., Edmonds, J., Kainuma, M., Riahi, K., Thomson, A., Hibbard, K., Hurtt, G.C.,

575 Kram, T., Krey, V., Lamarque, J.-F., Masui, T., Meinshausen, M., Nakicenovic, N., Smith, S.J.

576 and Rose, S.K.: The representative concentration pathways: an overview, Climatic Change, 109,

577 1-2, 5-31, doi: , 10.1007/s10584-011-0148-z, 2011.

578 Walcek, C.J., Brost, R.A., Chang, J.S., and Wesley, M.L., SO2, sulfate and HNO3 deposition

579 velocities computed using regional landuse and meteorological data, Atmospheric Environment,

580 20, 949-964, 1986.

581 Walmsley, J. L. and Wesely, M. L.: Modification of coded parametrizations of surface resistances

582 to gaseous dry deposition, Atmos. Environ., 30, 1181–1188, 1996.

583 Wesely, M.L.: Parameterization of surface resistances to gaseous dry deposition in regional-scale

584 numerical models, Atmos. Environ., 23, 6, 1293-1304, doi: 10.1016/0004-6981(89)90153-4,

585 1989.

586 Wesely, M.L. and Hicks, B.B.: A review of the current status of knowledge on dry deposition,

587 Atmos. Environ., 34, 2261 2282, doi: 10.1016/S1352-2310(99)00467-7, 2000.Zhang, L.M.,

588 Brook, J.R. and Vet, R.: On ozone dry deposition - with emphasis on non-stomatal uptake and

589 wet canopies, Atmos. Environ., 36, 30, 4787-4799, doi: 10.1016/S1352-2310(02)00567-8, 2002a.

590 Wu, S., Mickley, L. J., Kaplan, J. O., and Jacob, D. J.: Impacts of changes in land use and land

591 cover on atmospheric chemistry and air quality over the 21st century, Atmos. Chem. Phys., 12,

592 1597–1609, doi:10.5194/acp-12-1597-2012, 2012.

593 Zhang, L.M., Moran, M.D., Makar, P.A., Brook, J.R. and Gong, S.L.: Modelling gaseous dry

594 deposition in AURAMS: a unified regional air-quality modelling system, Atmos. Environ., 36, 3,

595 537-560, doi: 10.1016/S1352-2310(01)00447-2, 2002b.

596 Zhang, L., Brook, J. R., and Vet, R.: A revised parameterization for gaseous dry deposition in air-

597 quality models, Atmos. Chem. Phys., 3, 2067-2082, doi:10.5194/acp-3-2067-2003, 2003.

598

599 Table 1 : Simulations performed in our study with the LMDz-INCA chemistry-climate model : set-up description.

600

Run objectives	Land-cover map	Climate	Duration
CONTROL	Present-day 2000s	Winds and surface temperature nudged on ECMWF fields for 2007	1 year
IMPACT OF FUTURE LAND-USE CHANGES	2050 RCP 8.5	Winds and surface temperature nudged on ECMWF fields for 2007	1 year
	2050 RCP 4.5		
	2050 RCP 2.6		
IMPACT OF FUTURE CLIMATE	Present-day 2000s	2000-2010 fields (GCM mode)	10 years
		2045-2055 fields (GCM mode)	

601

602
603
604
605
606 Table 2 : Mean Effect on Annual Mean Surface Deposition Velocity (%) of climate and land cover changes of O_3 and
607 HNO_3 averaged over homogeneous regions (values > +-1.5% are highlighted)
608

	Ozone			Nitric Acid		
	Climate Change	RCP4.5 Land cover Change	Sum of Climate and Land cover Changes	Climate Change	RCP4.5 Land cover Change	Sum of Climate and Land cover Changes
GLOBAL	0.5	-0.7	-0.2	**2.2**	1.2	**3.4**
Eurasia	**2.1**	**-2.1**	0.0	**4.3**	**3.8**	**8.1**
USA	**1.5**	-1.3	0.2	**3.6**	**2.0**	**5.6**
Central America	-1.1	-1.4	**-2.6**	1.1	**1.7**	**2.8**
Tropical Southern America	**-2.3**	-1.2	**-3.5**	1.1	**2.6**	**3.7**
Tropical Africa	**-1.5**	-0.8	**-2.3**	0.4	0.9	1.3
South Africa	-1.4	-0.6	**-2.0**	-0.1	0.8	0.8
West Australia	-0.4	-0.1	-0.5	-0.4	0.0	-0.4
East Australia	-0.5	-0.6	-1.1	0.2	0.5	0.7
South America	0.4	-0.7	-0.4	0.3	**2.0**	**2.3**
Tropics	-1.1	-0.6	**-1.7**	0.6	1.0	**1.7**

609
610
611
612

23

613
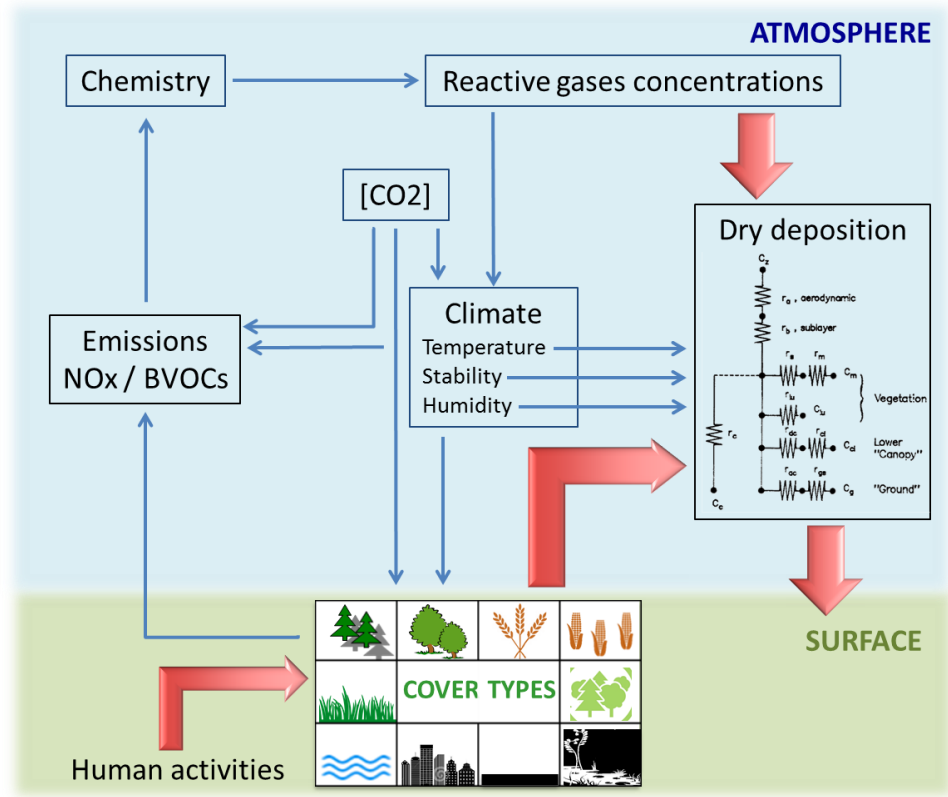
Figure 1: Interactions between vegetation and atmospheric chemistry potentially affected by land use changes. In this

work, only the red arrows are investigated.

616

617

618

619

620

621

622

623
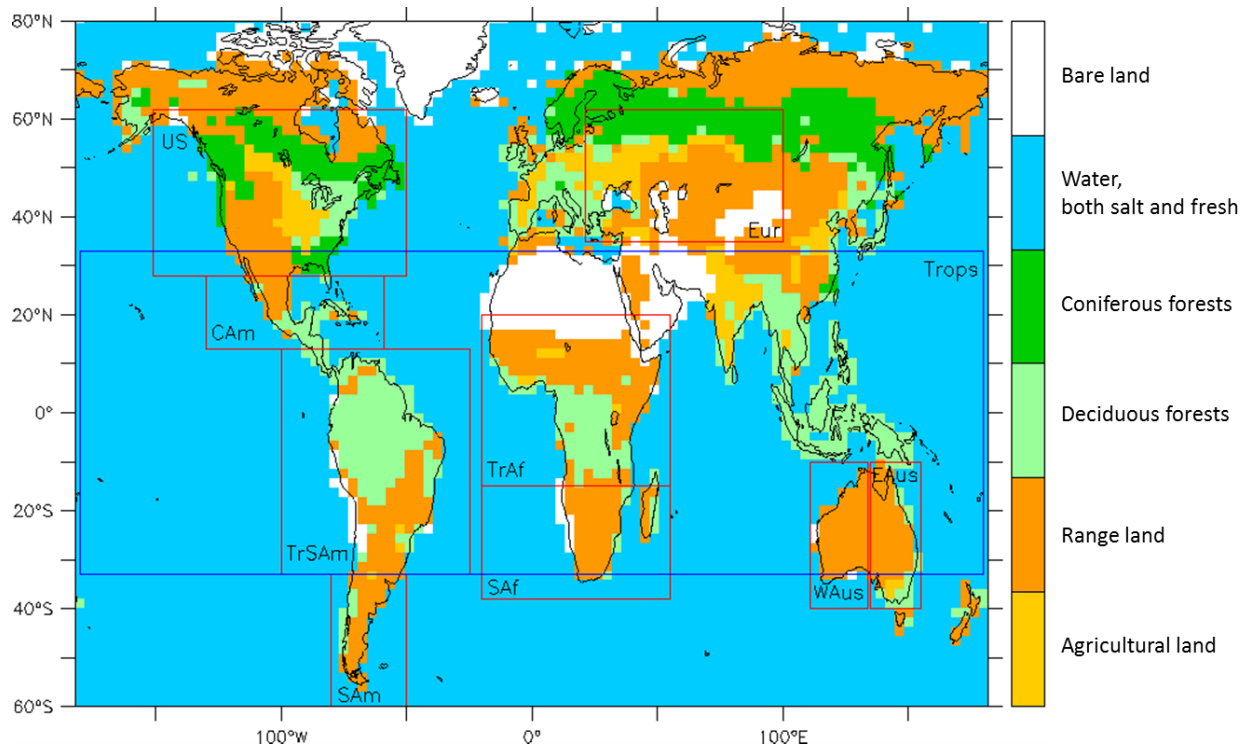
Figure 2: Surface categories considered in LMDz-INCA for dry deposition, represented as dominant coverage :
agricultural land, range land, deciduous forest, coniferous forest, water, barren land, mostly desert. Regions discussed
in this study are also illustrated: Eurasia, USA, Central America, Tropical Southern America, Southern America,
Tropical Africa, Southern Africa, Western Australia, Eastern Australia and Tropical regions.
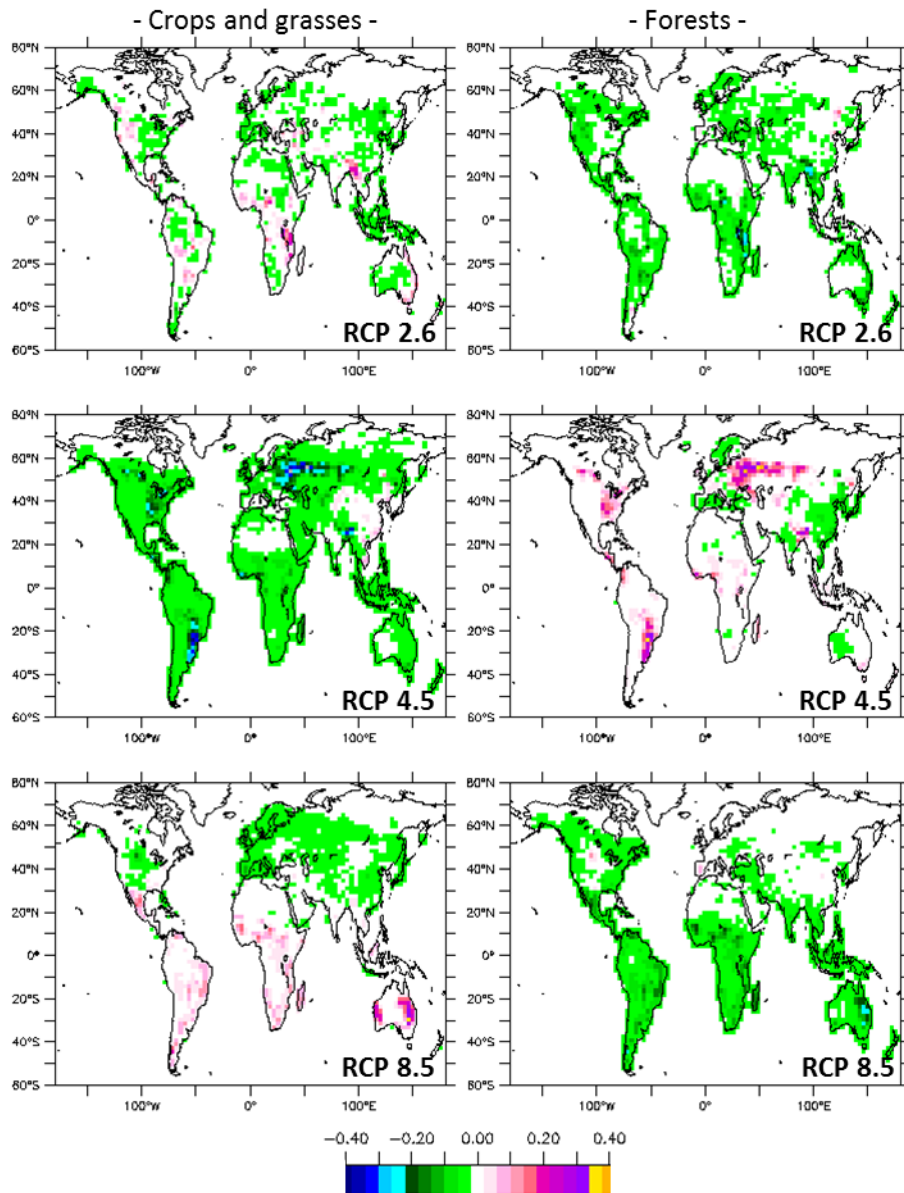
Figure 3: Vegetation fraction difference between 2050 and present-day for crops and grasses (left column), and forests (right column) according to the future RCP scenarios 2.6 (upper line), 4.5 (middle line) and 8.5 (lower line).

637
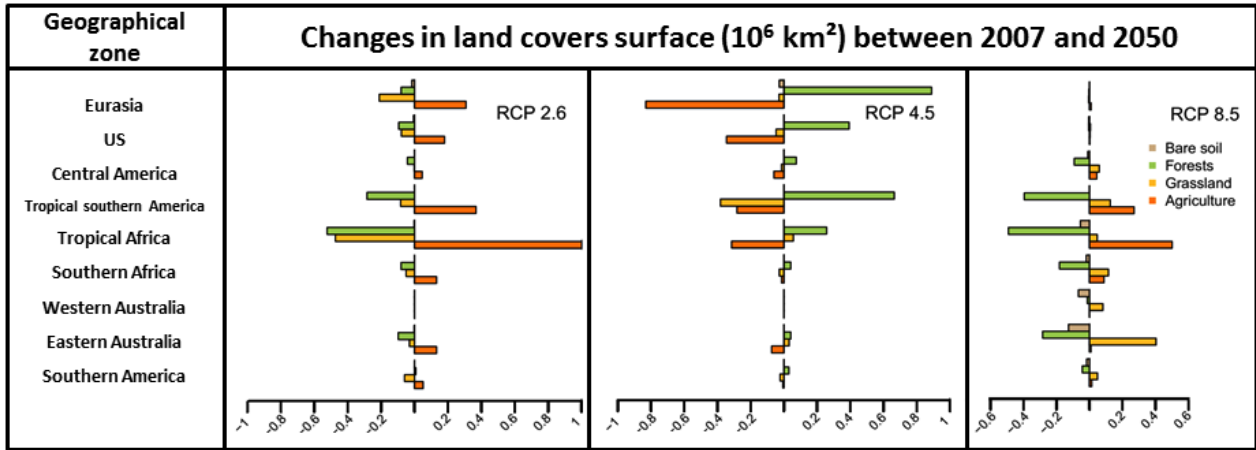
Figure 4: Changes between 2007 and 2050 in land-type surfaces (10^6 km²) for the nine regions as illustrated in figure 1, in the case of forests (green), crops (orange), grasses (yellow) and bare soil (brown).

639
640

641
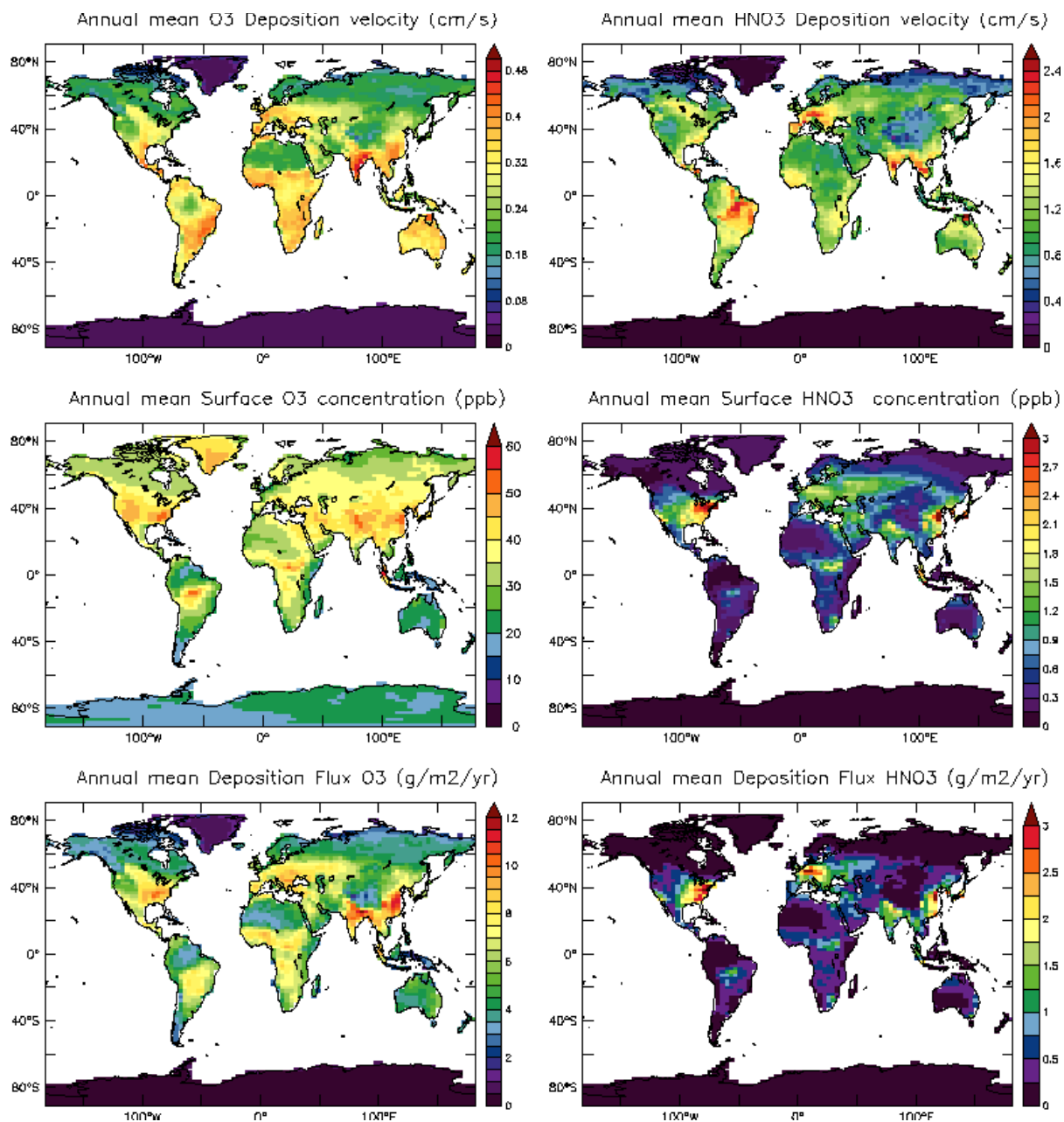
Figure 5: Annual average of surface dry deposition velocities (upper panel), surface concentrations (middle panel and deposition fluxes (lower panel) over continental surfaces (cm/s) for O_3 (left) and HNO_3 (right) for present-day as simulated by LMDz-INCA.
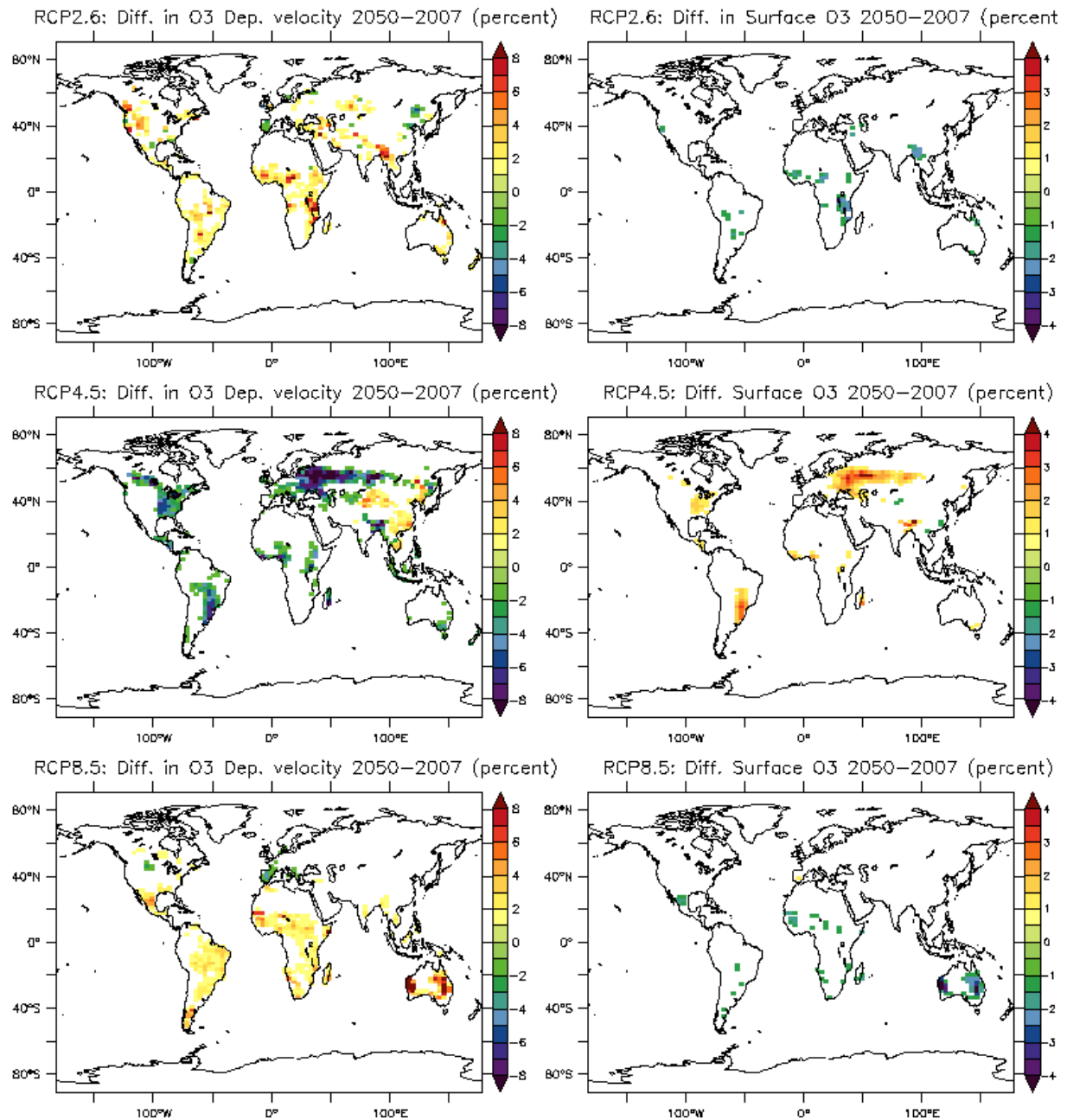
Figure 6: Annual mean changes (in relative value %) of surface dry deposition velocity for O$_3$ between present-day and 2050 induced by the different LCC (Left) and related surface ozone concentrations (Right) for the three RCP scenarios. Values in the [-1;+1]% interval are not shown
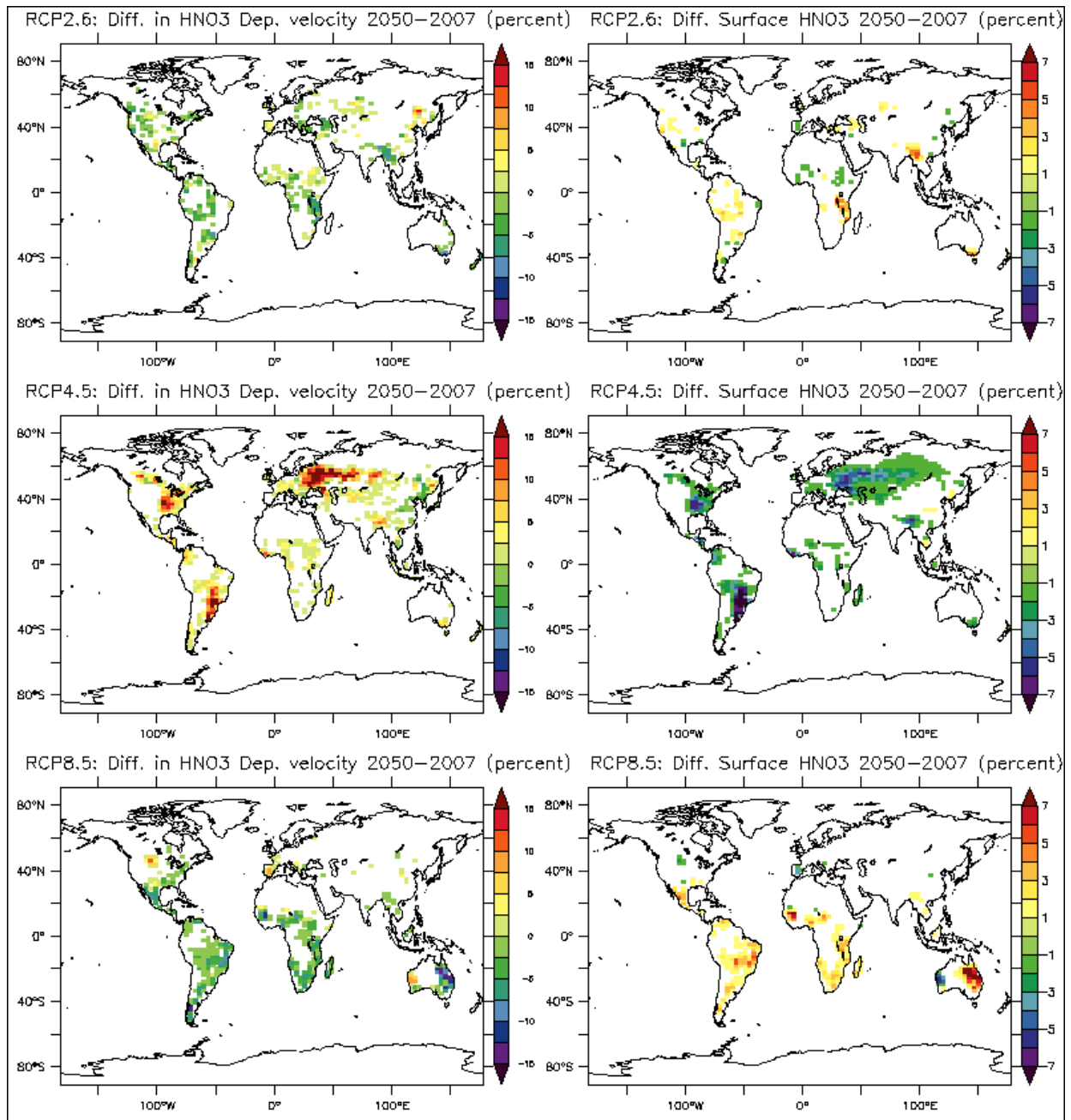
653

654   Figure 7: Same as Figure 6 for HNO₃.

655

656

657

658
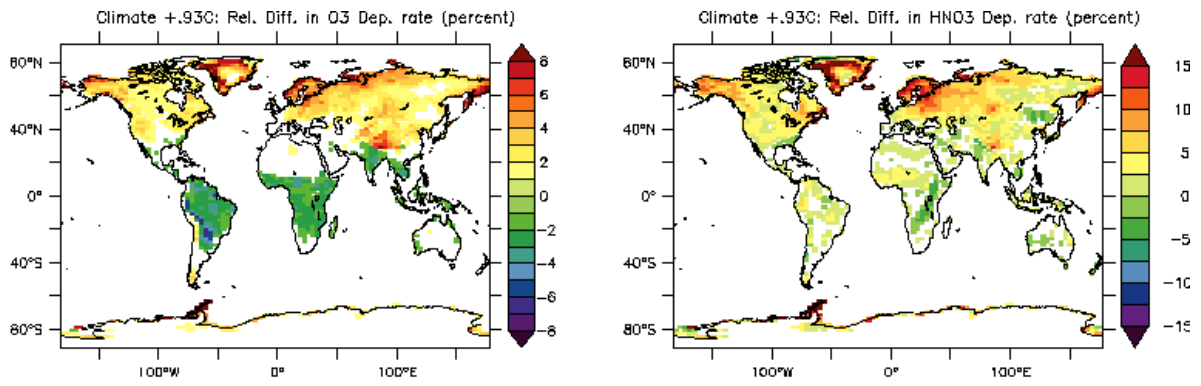
663 Figure 8: Future climate-induced impacts on surface dry deposition velocities (%) considering a 0.93°C increase of
664 global temperature.